Hindawi
International Journal of Antennas and Propagation
Volume 2017, Article ID 2961090, 8 pages
https://doi.org/10.1155/2017/2961090

*Research Article*

# Attenuation by a Human Body and Trees as well as Material Penetration Loss in 26 and 39 GHz Millimeter Wave Bands

**Qi Wang,[1] Xiongwen Zhao,[1,2,3] Shu Li,[1] Mengjun Wang,[2] Shaohui Sun,[2] and Wei Hong[3]**

[1]*School of Electrical and Electronic Engineering, North China Electric Power University, Beijing 102206, China*
[2]*State Key Laboratory of Wireless Mobile Communications, China Academy of Telecommunications Technology (CATT), Beijing 100191, China*
[3]*State Key Laboratory of Millimeter Wave, Southeast University, Nanjing 210096, China*

Correspondence should be addressed to Xiongwen Zhao; zhaoxw@ncepu.edu.cn

Received 13 October 2016; Revised 13 March 2017; Accepted 20 March 2017; Published 28 March 2017

Academic Editor: Stefan R. Panic

Copyright © 2017 Qi Wang et al. This is an open access article distributed under the Creative Commons Attribution License, which permits unrestricted use, distribution, and reproduction in any medium, provided the original work is properly cited.

This paper investigates the attenuation by a human body and trees as well as material penetration loss at 26 and 39 GHz by measurements and theoretical modeling work. The measurements were carried out at a large restaurant and a university campus by using a time domain channel sounder. Meanwhile, the knife-edge (KE) model and one-cylinder and two-cylinder models based on uniform theory of diffraction (UTD) are applied to model the shape of a human body and predict its attenuation in theory. The ITU (International Telecommunication Union) and its modified models are used to predict the attenuation by trees. The results show that the upper bound of the KE model is better to predict the attenuation by a human body compared with UTD one-cylinder and two-cylinder models at both 26 and 39 GHz. ITU model overestimates the attenuation by willow trees, and a modified attenuation model by trees is proposed based on our measurements at 26 GHz. Penetration loss for materials such as wood and glass with different types and thicknesses is measured as well. The measurement and modeling results in this paper are significant and necessary for simulation and planning of fifth-generation (5G) mm-wave radio systems in ITU recommended frequency bands at 26 and 39 GHz.

## 1. Introduction

Attenuation by a human body and trees and penetration loss of material at the ITU proposed frequency bands [1], 24.25–27.5 and 37–40.5 GHz, are important issues for future 5G (fifth-generation) wireless access systems. In this paper, attenuation by a human body and trees and penetration loss of different materials with 1 GHz bandwidth were measured with time domain channel sounder at 26 and 39 GHz, respectively. As far as we know, there are no measurements and modeling work reported in open literature on human blockage, attenuation by trees, and penetration loss of different materials at 24.25–27.5 and 37–40.5 GHz frequency bands. The prediction of attenuation by a human body and trees and the penetration loss in this work are important and necessary for future mm-wave wireless communication systems.

By considering a human body as an infinite absorbing screen, KE model was used to predict the attenuation by a person in a frequency range from 4 to 10 GHz in [2]. In addition, measurements in [3] showed that double knife-edge approach was suitable for both 60 GHz and 300 GHz bands. In addition to regarding a human body as an absorbing screen, a cylindrical model by uniform theory of diffraction (UTD) was also applied to predict human body attenuation. Measurements in [4, 5] were performed at 10 GHz which showed a strong correlation between a human body and a perfect conducing cylinder. By comparison with measurements at 60 GHz [6], it is shown that the UTD model was clearly overestimating the human attenuation.

In [7], measurements by a single tree were taken at a frequency range between 7.25 and 8.0 GHz and the attenuation by a tree is between 15 dB and 23 dB. In [8], measurements were taken at 9.6 GHz, 28.8 GHz, 57.6 GHz, and 96.1 GHz, and the results show that the vegetation loss increases nearly linearly at a range rate from 1.3 to 2.0 dB per meter. The ITU-R P-833-8 [9] proposes a model for the range from 30 MHz to 60 GHz: an exponential slant path model with elevation angle correction. Other widely used penetration loss models

are the exponential models proposed in [10–12], which do not consider the factor of elevation and are said to present frequency application ranges up to 57.6, 95, and 40 GHz, respectively. However, the coefficients of these models have been mainly computed from limited sets of data measured at frequencies close to 2 GHz. Therefore, there is still a need for verification measurements to test their correctness and applicability for higher frequencies.

Previous literatures about penetration loss of material in millimeter wave bands focused on 28 GHz and 60 GHz. In [13], signals through a hollow plasterboard wall resulted in a penetration loss ranging between 5.4 dB and 8.1 dB. In [14], the measured penetration losses are 2 dB, 9 dB, and 35.5 dB at 60 GHz through a glass door, a plasterboard wall with metallic studs, and a wall with a metal-backed blackboard, respectively.

In this paper, the measurements of the attenuation by a human body and trees as well as penetration loss for material were carried out. Attenuation by a human body was measured with a person laterally crossing the transceiver connection line. The KE and UTD methods are used to predict human body's attenuation. When using UTD, the human body was regarded as a cylinder and a combined model, respectively. In the combined model, the shoulders are regarded as two cylinders. By comparisons with different human models, the target is to get a better model to predict human body's attenuation at 26 and 39 GHz. In addition, we have measured the attenuation by willow trees at 26 GHz, and then the ITU-R P-833-8 model is modified by comparison with the measurement results. Measurements of the penetration loss for different materials were carried out in this work as well, for example, transparent glass with different thickness, frosted glass, and wood with plastic cladding.

The remainder of this paper is organized as follows. In Section 2, the measurement campaigns are introduced. In Section 3, attenuation models by a human body including KE and UTD one-cylinder and UTD two-cylinder models as well as the attenuation model by trees in ITU-R P-833-8 are investigated. Section 4 presents the measurement results with the comparisons of the models. Finally, we conclude the work in this paper in Section 5.

## 2. Measurement Campaigns

*2.1. Attenuation by a Human Body and Trees.* Channel measurements of the attenuation by a human body and trees were conducted at KeySight, Beijing office, and in the campus of North China Electric Power University, respectively. Table 1 lists the detailed specification of the system.

Figure 1 shows the measurement environment at a restaurant with more than 150 $m^2$ for human body attenuation. The heights of the transmitter (Tx) and receiver (Rx) are both 1.3 m above the ground level with distance of 15 meters.

The attenuation was measured with a person laterally crossing the Tx-Rx connection line as shown in Figure 2. When doing the measurement, the person was moving from −0.5 to 0.5 m crossing the Tx-Rx connection line with 2.5 cm distance step. Because of the sounding system limitation, the continuous measurement with time is not possible; the measurement had to be done with the human blocker moving step by step in different positions. The received power was measured when the Tx and Rx were placed in free space and the person was at fixed positions. In each position, the measurement was done 10 times (human blocker adjusting their positions 10 times as well); then the mean received power was calculated to prevent position randomness, rare moving scatterers occurring during the measurements, and the instability of the measurement system. The shoulder width of the measured person is 0.49 m, and thicknessof the body is 0.24 m. The human body attenuation was measured at both 26 and 39 GHz, respectively.

Figure 3 shows the measurement environment for trees attenuation at 26 GHz; 1–4 willow trees were measured between the Tx and Rx with the heights of 6.0 m and 2.0 m, respectively. The height of the willow trees is about 14 m. The tree radius is about 3 m with sparse branches and leaves. An omnidirectional biconical horn with 3 dBi gain was used at the Tx, and a 26 dBi horn with the height of 2 m was applied at the Rx and rotated just in the elevation plane with azimuth

Table 1: Specification of the system.

| Parameter | 26 GHz | 39 GHz |
|---|---|---|
| Bandwidth | 1 GHz | 1 GHz |
| Maximum delay | 1.024 us | 1.024 us |
| Delay resolution | 1 ns | 1 ns |
| Tx power | 24 dBm | 24 dBm |
| Heights of the Tx/Rx | 1.3/1.3 m (human)<br>6.0/2.0 m (tree) | 1.3/1.3 m (human)<br>6.0/2.0 m (tree) |
| Gain of the horn antenna | 24.3 dBi | 27 dBi |
| Polarization of the horn antenna | Vertical | Vertical |
| HPBW of the horn antenna | 10° | 10° |

Figure 1: Measurement environment for human attenuation.

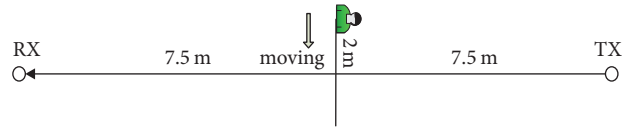


Figure 2: A person laterally crossing the Tx-Rx connection line.

Figure 3: Measurement environment for tree attenuation.

angle of 0°. The 0° direction in the azimuth plane points to the Tx. At locations 1 and 2, the horn was rotated in the elevation plane from 10° to 50° with a step of 10°, while at locations 3 and 4, the horn was rotated in elevation plane from 10° to 40° and from 10° to 30° with a step of 10°, respectively. When doing the measurements, the Rx was placed in the middle of the two adjacent trees.

*2.2. Penetration Loss of Different Materials.* Penetration loss for different materials was measured at KeySight office in Beijing. The received power was measured when the transceiver was in free space and the tested material was placed in the middle of the transceiver; then the power difference is defined as the penetration loss of the material.

Figure 4 shows the measurement scenarios for tested materials. The wood and glass with different thickness and surface were measured. In Figure 4(a), it is a wooden door with painting. In Figure 4(d), it is a wooden door with plastic cladding. Two kinds of glass are measured: one is transparent glass shown in Figure 4(b) and the other is frosted glass shown in Figure 4(c). In addition, there are two transparent glass doors in the hall; the penetration losses through one door and two doors were measured, respectively.

Transmit power was set from 0, 10, and 20 dBm in each measurement; the channel impulse responses were recorded 10 times with same transmit power. Finally, the mean penetration loss with different transmit power is calculated to avoid possible instability of the measurement system.

## 3. Models of Attenuation by a Human Body and Trees

### 3.1. Attenuation Models by a Human Body

*3.1.1. Double Knife-Edge Model.* In this model, a human body is regarded as an absorbing screen with infinite height, where shoulders are regarded as two knife edges. Figure 5 shows the geometry of the two knife edges, where $h_a$ and $h_b$ are the widths for the left and right human shoulders. $d_T$ and $d_R$ are the distances from the Tx and Rx to the human, respectively. The diffraction field $A_S$ is the sum of two knife edges, which is given by

$$A_S[h_a, h_b] = A_H[h_a] + A_H[h_b]. \quad (1)$$

The diffraction field $A_H$ can be calculated as

$$A_H = \frac{U_H}{U_0} = \frac{1+j}{2}\left\{\left(\frac{1}{2} - C(\nu)\right) - j\left(\frac{1}{2} - S(\nu)\right)\right\}, \quad (2)$$

where $U_H$ and $U_0$ denote the diffracted field and the field in absence of an obstruction, respectively.

$C(\nu) + jS(\nu) = \int_0^{\nu} \exp(j\pi t^2/2)d\nu$ is the Fresnel integral, and

$$\nu(h) = h\sqrt{\frac{2}{\lambda}\frac{d_T + d_R}{d_T d_R}} \quad (3)$$

is relative to wavelength $\lambda$, obstruction depth $h$, and distance parameters.

*3.1.2. One-Cylinder Model.* In addition to the knife-edge models aforementioned, UTD model has been applied to predict the attenuation by human body as well, in which a human body is regarded as a cylinder. Figure 6 shows a cylinder model with radius of $\alpha$. Point $S$ is the source position. Points $P$ and $\widetilde{P}$ are the observation positions, respectively, in the shadow and illuminated regions. $Q_R$ in Figure 6 is the reflection point, while $S_{d1}$~$S_{d4}$ are the diffraction points.

As shown in Figure 6, when the observation point $\widetilde{P}$ is in the illuminated region, the total received field is the sum of the reflected field from the human body and the incident field in case the person does not block the Tx-Rx connection line with lateral crossing. When the person blocks the Tx-Rx connection line, the receiver appears to be in the shadow region and the diffracted fields from both sides of the human body contribute to the total received field.

The incident field of observation point $\widetilde{P}$ can be expressed as

$$E^i(r) = E^i(r_0)\sqrt{\left(\frac{\rho_1^i}{\rho_1^i + s^i}\right)\left(\frac{\rho_2^i}{\rho_2^i + s^i}\right)}e^{-jks^i}, \quad (4)$$

where $\rho_1^i$ and $\rho_2^i$ are the radii of curvatures of the incident wavefront. $r_0$ is the reference point, and $s^i$ is the distance along the incident ray from $r_0$ to reference point $r$. $k$ is wave number. Equation (4) can be simplified further to (5)–(7) if the incident wave is assumed as plane wave, spherical wave, and cylindrical wave, respectively:

$$E^i(r) = E^i(r_0)e^{-jks^i}, \quad (5)$$

$$E^i(r) = \frac{E^i(r_0)e^{-jks^i}}{s^i}, \quad (6)$$

$$E^i(r) = \frac{E^i(r_0)e^{-jks^i}}{\sqrt{s^i}}. \quad (7)$$


FIGURE 4: Penetration loss measurements for a wooden door of the laboratory (a), a transparent glass door of the hall (b), a frosted glass door of a small office (c), and a wooden door of the cabinet (d).

The reflected field is calculated by

$$E^r(P) = E^i(Q_R)\,\overline{\overline{R}}\sqrt{\left(\frac{\rho_1^r}{\rho_1^r + s^r}\right)\left(\frac{\rho_2^r}{\rho_2^r + s^r}\right)}e^{-jks^r}, \quad (8)$$

where $\rho_1^r$ and $\rho_2^r$ are the radii of curvatures of the reflected wave and $\overline{\overline{R}}$ includes hard reflection coefficients $R_h$ and soft reflection coefficients $R_s$.

The reflection coefficient is defined as

$$R_{s,h} = -\left[\sqrt{\frac{-4}{\xi^L}}e^{-j(\xi^L)^3/12}\left\{\frac{e^{-j(\pi/4)}}{2\sqrt{\pi}\xi^L}\left[1 - F\left(X^L\right)\right] + \widehat{P}_{s,h}\left(\xi^L\right)\right\}\right], \quad (9)$$

where $\xi^L$ and $X^L$ are expressed in [15].

The diffracted field is

$$E^d(P) = E^i(S_{d1})\,\overline{\overline{T}}\sqrt{\frac{\rho_2^d}{s^d\left(\rho_2^d + s^d\right)}}e^{-jks^d}, \quad (10)$$

when $P$ is located in shadow region.

$$\rho_2^d = s_0 + t,$$
$$\overline{\overline{T}}_{s,h} = -\left[\sqrt{m(S_{d1})\,m(S_{d2})}\sqrt{\frac{2}{k}}\left\{\frac{e^{-j(\pi/4)}}{2\sqrt{\pi}\xi^d}\left[1 - F\left(X^d\right)\right] + \widehat{P}_{s,h}\left(\xi^d\right)\right\}\right]\sqrt{\frac{s_0}{s_0 + t}}e^{-jkt}, \quad (11)$$

where $t$ is the distance between two diffraction points. $s_0$ is the distance between the source and the first diffraction point $S_{d1}$, and $s^d$ is the distance between the second point $S_{d2}$ and $P$. The "Transition" function $F(X)$, "Pekeris" function, and other parameters can be found in [15–17].

Table 2: Summary of the maximum attenuation of the measurement and the upper bound of the KE, one-cylinder, and two-cylinder models.

| Frequency | The maximum attenuation (dB) | | | |
|---|---|---|---|---|
| | Measurement | KE model (upper bound) | One-cylinder model (upper bound) | Two-cylinder model (upper bound) |
| 26 GHz | 12.66 | 11.51 | 14.25 | 17.89 |
| 39 GHz | 19.03 | 13.46 | 15.66 | 19.99 |

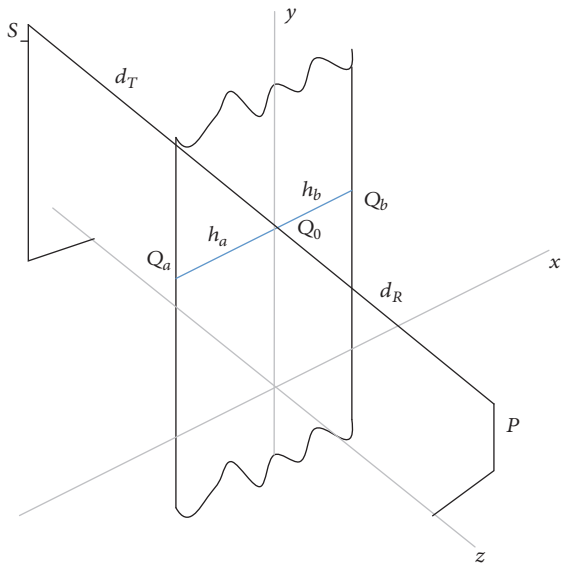


Figure 5: Double knife-edge model.

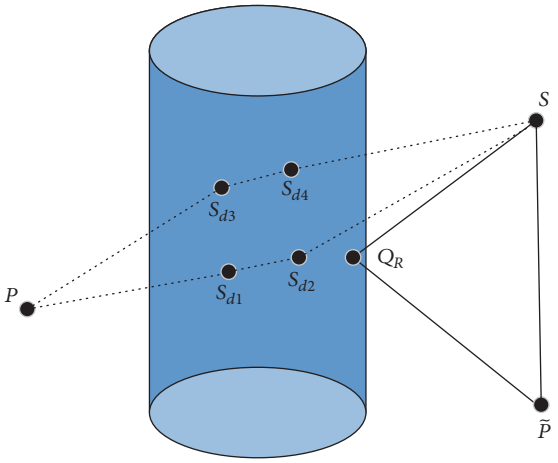


Figure 6: One-cylinder model.

*3.1.3. Two-Cylinder Model.* Two-cylinder model is based on one-cylinder model; instead of regarding a person as a whole cylinder, the shoulders are regarded as two cylinders with smaller radii as shown in Figure 7.

*3.2. Attenuation Models by Trees.* According to ITU-R P-833-8 [9], attenuation by trees can be expressed as

$$L = A \cdot f^B d_v{}^C \theta^D \text{ dB}, \tag{12}$$

where $f$ is the carrier frequency in MHz, $d_v$ is the penetration distance of the trees between transmitter and receiver, $\theta$ is the elevation in degrees, and $A$, $B$, $C$, and $D$ are empirical constants.

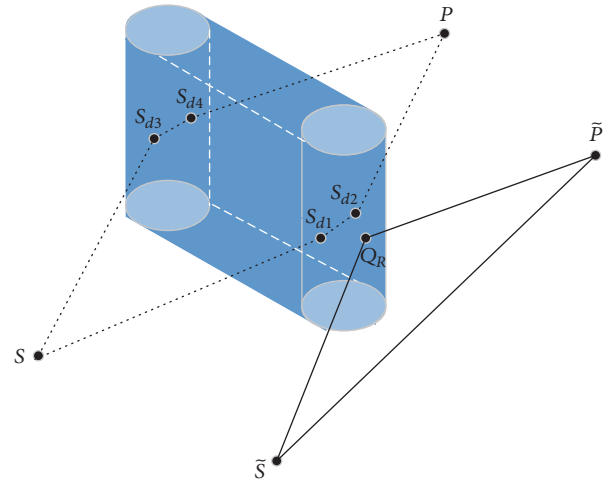


Figure 7: Two-cylinder model.

## 4. Measurement Results and Analysis

*4.1. Attenuation by a Human Body and Trees.* In the measurements, no moving scatterers existed close to the transceiver. The heights of the transceiver as well as the distance between transmitter and receiver were planned in detail to avoid reflection from the ground, especially in human blockage measurement with smooth ground. Because of very narrow beamwidth of the horn antennas, multipath from fixed scatterers can also be avoided. Therefore, the attenuation is essentially the diffraction loss around the blocker(s). When doing the measurements, at first, the CIRs were measured in free space; then the CIRs were recorded with the blocker(s). The noise floor was decided by averaging the last 200 delay samples, and we use 5 dB higher than the noise floor to remove the noise due to its fluctuation. The human attenuation was defined as the difference of the wideband received powers which was measured in free space and measured with human blocker.

Figures 8(a) and 8(b) are the comparisons between the measurements and theoretical models at 26 and 39 GHz, respectively. Table 2 summarizes the maximum attenuation of the measurements and the maximum attenuation of the upper bound of KE and one-cylinder and two-cylinder models at 26 and 39 GHz, respectively. In Figure 8(a), compared to the upper bound of one-cylinder and two-cylinder models, the measurement result agrees better with the upper bound of the KE model. The field fluctuation in shadowing

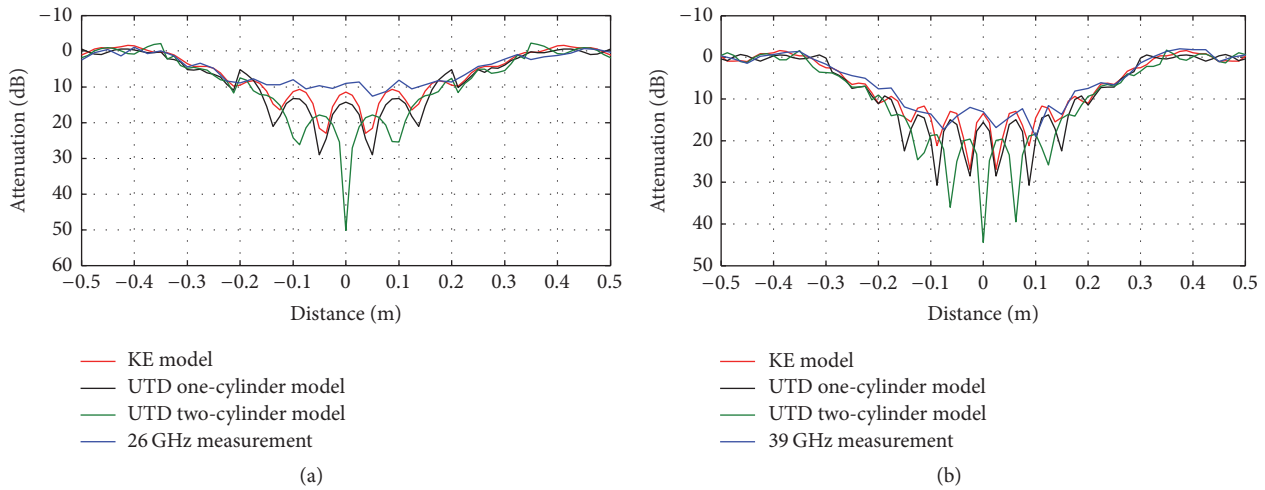


Figure 8: Comparison between the measurement and models: (a) 26 GHz and (b) 39 GHz.

region is obviously observed in the KE and one-cylinder and two-cylinder models due to the superposition of the field from both sides of the models in a coherent manner. The fluctuation intensity is very sensitive to the wavelength and measurement configurations. The maximum attenuation of measurement is 12.66 dB. If we just consider the upper bound values of models, the maximum attenuation of the KE and one-cylinder and two-cylinder models is 11.51, 14.18, and 18.32 dB, respectively, as shown in Table 2. The RMSEs are 1.97 dB, 2.50 dB, and 2.97 dB between measurements and the three models at 26 GHz, respectively. In Figure 8(b), the maximum attenuation of the measurement is 19.03 dB and it is close to the upper bound of two-cylinder model as shown in Table 2. The RMSEs are 2.01 dB, 2.40 dB, and 2.89 dB between measurements and KE and one-cylinder and two-cylinder models at 39 GHz, respectively. As a whole, the measurements agree better with the KE model at 26 and 39 GHz in the shadow region. Two-cylinder model might be more like the human body, but it overestimates the attenuation by numerical calculation. In addition, the KE model is concise; therefore it is good to be used to predict the human blockage effect at 26 and 39 GHz in a practical use case.

If the shape of a human body is neglected, we can use measured attenuation only to get more simple models with respect to distances at 26 and 39 GHz. Figure 9 shows the attenuation models based on measurements. Formulas 4.1 are the empirical piecewise functions for human attenuation at 26 and 39 GHz. When the human does not block the Tx and Rx connection line, the attenuation fluctuates around zero dB.

$$
\begin{aligned}
-0.5 \times d + 0.1 \quad & d < -\frac{W}{2}, \\
-128 \times d^2 - 0.1 \times d + 10.6 \quad & -\frac{W}{2} \le d \le \frac{W}{2}, \\
-4.7 \times d + 2.4 \quad & d > \frac{W}{2}, \\
-11.5 \times d - 4.2 \quad & d < -\frac{W}{2},
\end{aligned}
$$

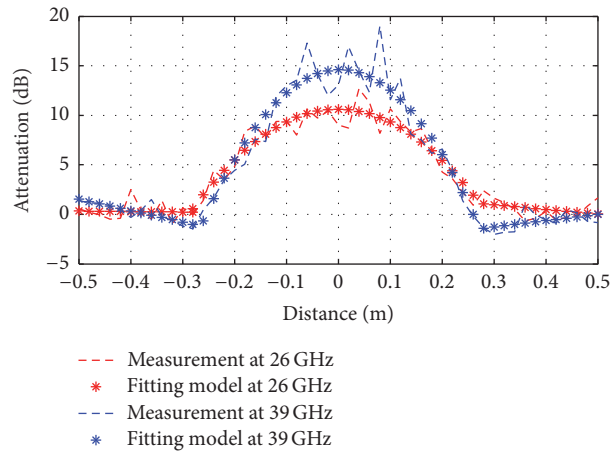


Figure 9: Simplified human attenuation models by measurements at 26 GHz and 39 GHz.

$$
\begin{aligned}
-221 \times d^2 + 1.3 \times d + 14.6 \quad & -\frac{W}{2} \le d \le \frac{W}{2}, \\
6.4 \times d - 3.2 \quad & d > \frac{W}{2},
\end{aligned}
\tag{13}
$$

where $W$ is the width of the human and $d$ is the distance.

When measuring the attenuation by trees, the horn antenna was adjusted to point the trees with azimuth angle of 0°; then the horn was rotated in the elevation plane to measure the attenuation from different parts of the trees. In the following text, measurement locations 1–4 are with respect to 1–4 trees, respectively. At locations 1 and 2, the horn was rotated in the elevation plane from 10° to 50° with a step of 10°, while at locations 3 and 4, the horn was rotated in elevation plane from 10° to 40° and from 10° to 30° with a step of 10°, respectively. Based on the transceiver distance and height difference of the transmitter and receiver, the elevation angles of the direct rays are 31.62°, 18.58°, 12.88°, and 10.26°, respectively, for locations 1 to 4.

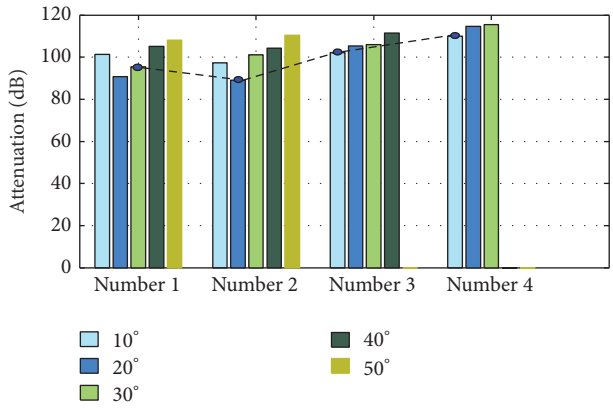


Figure 10: Measured attenuation by 1–4 trees with different elevation angles.

Table 3: Attenuation by 1–4 willow trees.

| Location | 1 | 2 | 3 | 4 |
|---|---|---|---|---|
| Attenuation (dB) | 18.50 | 12.80 | 15.54 | 22.42 |

Figure 10 shows the attenuation by 1–4 trees, respectively, including free space path loss in different elevation angles. Numbers 1–4 mean locations 1–4. The dashed line shows attenuation of the direct rays by the tree(s). The elevation angles for the direct rays by 1–4 trees are different because of different distances between transmitter and receiver.

We define here the attenuation by tree(s) as the difference between the attenuation of the direct path of the tree(s) and the path loss in free space. Therefore, the attenuation by 1–4 willow trees is shown in Table 3.

At location 1, the attenuation of the 1st tree is 18.50 dB, a large attenuation caused by the trunk and leaves. At location 2, the attenuation is 12.80 dB caused by the branches and leaves of the 1st and 2nd trees with 1.22 dB/m attenuation in average according to the penetration distance of the trees. Sparse branches and leaves make the attenuation small.

At location 3, the attenuation is 15.54 dB. The direct path is blocked by the branches and leaves of the 1st to 3rd trees with 0.97 dB/m attenuation in average. At location 4, the attenuation is 22.42 dB in total. The direct path is blocked by the branches and leaves of the 1st to 4th trees with 1.10 dB/m attenuation in average.

Based on our measurements, in case the direct path was blocked by the branches and leaves, the average attenuation is within 0.97 to 1.22 dB per meter, which is affected by the density of the branches and leaves. In case the direct path was blocked by the trunk, the attenuation by a willow tree is up to 18.50 dB. Therefore, difference between the attenuation by the trunk and that by branches and leaves is observed. In this work, the latter case is taken into consideration.

In Rec. ITU-R P-833-8 [9], attenuation in vegetation was investigated by measurements done in pine woodland in Austria for satellite slant paths as expressed in Section 3.2 for the model with $A$–$D$ empirical parameters. The model for pin trees is expressed as follows:

$$L = 0.25 \cdot f^{0.39} \cdot {d_v}^{0.25} \cdot \theta^{0.05} \text{ dB}, \quad (14)$$

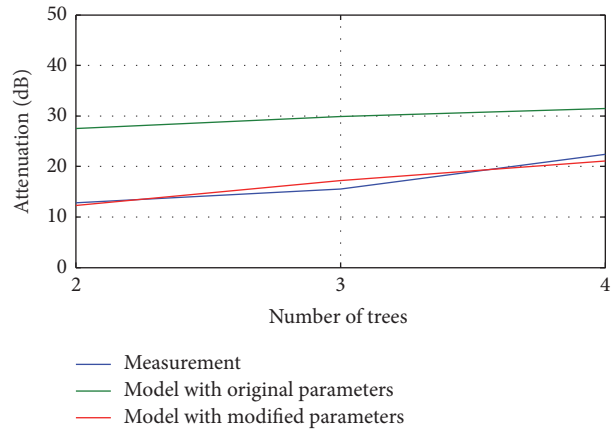


Figure 11: Comparison between the models and measurement.

where $A = 0.25$, $B = 0.39$, $C = 0.25$, and $D = 0.05$ are empirical parameters for (12). Figure 11 shows our measurement attenuation by the branches and leaves of willow trees in blue line; the attenuation of (14) for pin trees is in green line. It is seen that ITU model overestimates the attenuation of willow trees. ITU model may include the trunk attenuation inside with small elevation angles in satellite links. To use model (14) at 26 GHz, parameters in it need to be modified. In (14), parameter $D$ shows the relationship between the attenuation and elevation angles. When $D$ is positive, it means that the attenuation is proportional to an elevation angle. In fact, the branches and leaves in the upper part of the trees are more sparse and thinner than those in the lower part. Thicker branches and leaves make the attenuation larger; therefore the attenuation should grow inversely proportional to the elevation angles. Considering aforementioned reasons, (12) and (14) can be modified as follows:

$$\log(L) = 0.39 \cdot \log(A \cdot f) + 0.25 \cdot \log(d_v) + D \cdot \log(\theta) \text{ dB}, \quad (15)$$

where $A$ and $D$ are modified by measurement data at 26 GHz using least-square method; then (15) can be expressed as

$$L = 0.58 \cdot f^{0.39} \cdot {d_v}^{0.25} \cdot \theta^{-0.63} \text{ dB}. \quad (16)$$

It is seen from Figure 11 that the modified model (16) in red line agrees well with the measurement result.

*4.2. Penetration Loss of Different Materials.* Table 4 summarizes the penetration loss of different materials with specific thicknesses at 26 and 39 GHz, respectively. It is seen that the loss at 39 GHz is larger than that at 26 GHz for each material in general. From Table 4, it is found that the total thickness of the two transparent glass doors of the hall is 25.70 mm which is thinner than the wooden door of the laboratory, but their attenuation is almost the same; it means that wooden attenuation is smaller than that of transparent glass in the same thickness at 26 and 39 GHz, respectively. The wooden door of the cabinet is thinner than the wooden door of the laboratory; however, no big attenuation difference at 26 GHz

Table 4: Penetration losses of the materials.

| Material | Thickness | 26 GHz | 39 GHz |
|---|---|---|---|
| Wooden door of the laboratory | 47.94 mm | 5.50 dB | 9.69 dB |
| Transparent glass door of the hall (one door) | 12.85 mm | 3.95 dB | 4.59 dB |
| Transparent glass door of the hall (two doors) | 25.70 mm | 5.55 dB | 9.45 dB |
| Frosted glass door of the small office | 12.30 mm | 4.10 dB | 4.65 dB |
| Wooden door of the cabinet | 19.82 mm | 4.16 dB | 5.59 dB |

is found. In addition, penetration loss of the frosted glass door is slightly larger than that of transparent glass.

## 5. Conclusions

In this paper, attenuation by human body and trees and penetration loss of different materials at 26 and 39 GHz are investigated for 5G wireless communications. By comparisons of the KE model, one-cylinder model, and two-cylinder model with measured human attenuation, it is found that the KE model is compact and concise and is a better model to be applied. In addition, more accurate attenuation models by a human are developed based on measurement attenuation using linear regression method at 26 and 39 GHz, respectively. The attenuation by trees is also investigated in this work at 26 GHz. In case the direct path is blocked by the branches and leaves, the attenuation by willow trees is within 0.97~1.22 dB per meter. In case the direct path is blocked by the trunk, the attenuation by a tree is up to 18.50 dB. The material penetration loss measurements are focused on wooden and glass. It is found that the penetration loss for wood is smaller than that of transparent glass in the same thickness, and the penetration loss of frosted glass is slightly larger than that of transparent glass.

## Conflicts of Interest

The authors declare that they have no conflicts of interest.

## Acknowledgments

This work is supported by State Key Laboratory of Wireless Communications, China Academy of Telecommunications Technology (CATT), and the open research fund of State Key Laboratory of Millimeter Waves, Southeast University (no. K201517). It is also supported by the Fundamental Research Funds for the Central Universities (2015 XS19). Thanks are due to Mr. Zhu Wen, Fei Cao, and Tiansheng Zhang from KeySight, Beijing, for their great help in making the measurements.

## References

[1] ITU, in *Proceedings of the World Radio Communication Conference (WRC '15)*, ITU 500-E, Geneva, Switzerland, November 2015.

[2] J. Kunisch and J. Pamp, "Ultra-wideband double vertical knife-edge model for obstruction of a ray by a person," in *Proceedings of the IEEE International Conference on Ultra-Wideband (ICUWB '08)*, pp. 17–20, Hannover, Germany, September 2008.

[3] M. Jacob, S. Priebe, R. Dickhoff, T. Kleine-Ostmann, T. Schrader, and T. Kürner, "Diffraction in mm and sub-mm wave indoor propagation channels," *IEEE Transactions on Microwave Theory and Techniques*, vol. 60, no. 3, pp. 833–844, 2012.

[4] M. Ghaddar, L. Talbi, and T. A. Denidni, "Human body modelling for prediction of effect of people on indoor propagation channel," *Electronics Letters*, vol. 40, no. 25, pp. 1592–1594, 2004.

[5] M. Ghaddar, L. Talbi, T. A. Denidni, and A. Sebak, "A conducting cylinder for modeling human body presence in indoor propagation channel," *IEEE Transactions on Antennas and Propagation*, vol. 55, no. 11, pp. 3099–3103, 2007.

[6] M. Peter, M. Wisotzki, M. Raceala-Motoc et al., "Analyzing human body shadowing at 60 GHz: systematic wideband MIMO measurements and modeling approaches," in *Proceedings of the 6th European Conference on Antennas and Propagation (EuCAP '12)*, pp. 468–472, Prague, Czech, March 2012.

[7] L. E. Bråten and V. Arneson, "Measurements of single tree attenuation for vehicular satellite communications at X-band," in *Proceedings of the 8th European Conference on Antennas and Propagation (EuCAP '14)*, pp. 1264–1268, Hague, The Netherlands, April 2014.

[8] D. L. Jones, R. H. Espeland, and E. J. Violette, *Vegetation Loss Measurements at 9.6, 28.8, 57.6, and 96.1 GHz through a Conifer Orchard in Washington State*, U.S. Department of Commerce, 1989.

[9] ITU, "Attenuation in vegetation," Rec. ITU-R P.833-8, 2013.

[10] COST 235, "Radiowave propagation effects on next generation fixed services terrestrial telecommunications systems," Final Report, 1996.

[11] M. A. Weissberger, "An initial summary of models for predicting the attenuation of radio waves by trees," Tech. Rep. ESD-TR-81-101, Electromagnetic Compatibility Analysis Center, 1982.

[12] M. O. Al-Nuaimi and R. B. L. Stephens, "Measurements and prediction model optimisation for signal attenuation in vegetation media at centimetre wave frequencies," *IEE Proceedings—Microwaves, Antennas and Propagation*, vol. 145, no. 3, pp. 201–206, 1998.

[13] E. J. Violette, R. H. Espeland, R. O. DeBolt, and F. Schwering, "Millimeter-wave propagation at street level in an urban environment," *IEEE Transactions on Geoscience and Remote Sensing*, vol. 26, no. 3, pp. 368–380, 1988.

[14] K. Sato, T. Manabe, T. Ihara et al., "Measurements of reflection and transmission characteristics of interior structures of office building in the 60-GHz band," *IEEE Transactions on Antennas and Propagation*, vol. 45, no. 12, pp. 1783–1792, 1997.

[15] R. G. Kouyoumjian and P. H. Pathak, "A uniform geometrical theory of diffraction for an edge in a perfectly conducting surface," *Proceedings of the IEEE*, vol. 62, no. 11, pp. 1448–1461, 1974.

[16] P. H. Pathak, "An asymptotic analysis of the scattering of plane waves by a smooth convex cylinder," *Radio Science*, vol. 14, no. 3, pp. 419–435, 1979.

[17] N. A. Logan, *General Research in Diffraction Theory. Volume I LMSD-288087; and Volume II LMSD-288088*, Missiles and Space Division, Lockheed Aircraft Corporation, 1959.

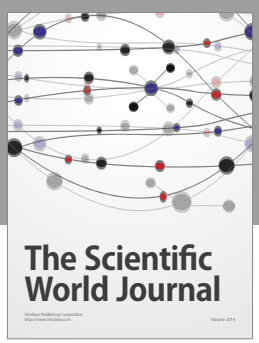

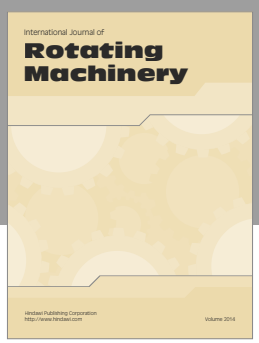

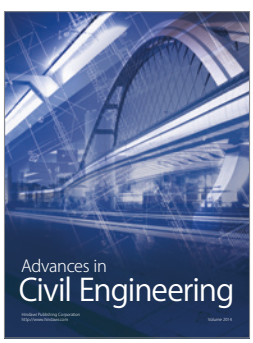

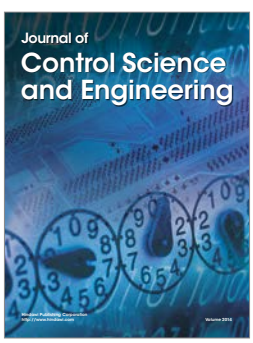

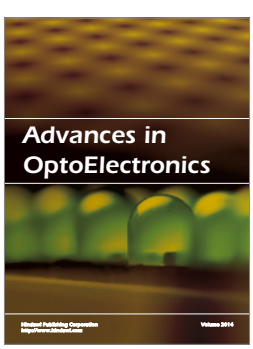

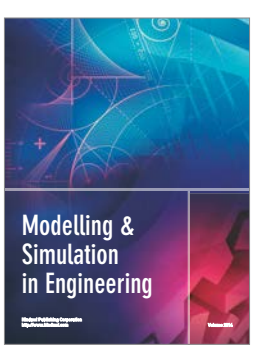

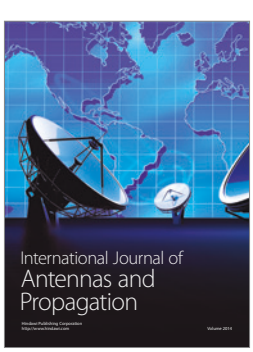

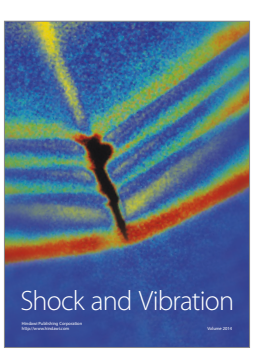

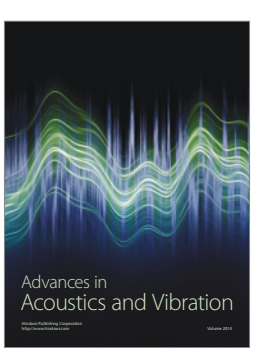

Hindawi

Submit your manuscripts at
https://www.hindawi.com